Check for updates

Multiscale real time and high sensitivity ion detection with complementary organic electrochemical transistors amplifier

Paolo Romele [1], Paschalis Gkoupidenis [2], Dimitrios A. Koutsouras[2], Katharina Lieberth[2], Zsolt M. Kovács-Vajna [1], Paul W. M. Blom [2] & Fabrizio Torricelli [1✉]

Ions are ubiquitous biological regulators playing a key role for vital processes in animals and plants. The combined detection of ion concentration and real-time monitoring of small variations with respect to the resting conditions is a multiscale functionality providing important information on health states. This multiscale functionality is still an open challenge for current ion sensing approaches. Here we show multiscale real-time and high-sensitivity ion detection with complementary organic electrochemical transistors amplifiers. The ion-sensing amplifier integrates in the same device both selective ion-to-electron transduction and local signal amplification demonstrating a sensitivity larger than 2300 mV V^{-1} dec^{-1}, which overcomes the fundamental limit. It provides both ion detection over a range of five orders of magnitude and real-time monitoring of variations two orders of magnitude lower than the detected concentration, viz. multiscale ion detection. The approach is generally applicable to several transistor technologies and opens opportunities for multifunctional enhanced bioelectronics.

[1] University of Brescia, Department of Information Engineering, via Branze 38, 25123 Brescia, Italy. [2] Max Planck Institute for Polymer Research, Ackermannweg 10, 55128 Mainz, Germany. ✉email: fabrizio.torricelli@unibs.it

ons are the ubiquitous biological and physiological regulators, being involved in most of the fundamental processes of every living organism. Ions enable the communication between cells and the vital metabolic and bioenergetic processes, playing a key role in hydration, pH regulation, and osmotic balance across cell membranes[1,2]. Ions regulate the operation of nerves, muscles, and neural signals in animals and the activation of enzymes, turgor, and photosynthesis in plants. As a consequence, life is permeated by a close connection with ions, and the ion concentration levels in biological systems can give important information on their state of health. For instance, an optimal ionic uptake of plants from the soil is fundamental to exploit their vital functions, but ionic excesses can be toxic[3,4]. Analogously, abnormal levels in human body fluids are often the fingerprint of ongoing pathological states and diseases[5], organ disfunctions such as heart or kidney failure, and dehydration[6]. Ion regulation in living organisms involves intra and extracellular fluctuations from the resting condition, which typically ranges from 10^{-4} M to 10^{-1} M, and small deviations from the optimal equilibrium levels can be associated with pathological states[7]. As an example, the normal potassium concentration in human serum is in the range from 3.5 10^{-3} to 5.5 10^{-3} M and a departure from this range lower than 20% can be associated with severe morbidity and mortality[8]. Analogously, during an epileptic seizure the neuronal extracellular concentration of potassium (K^+) increases from 4 10^{-3} M to 12 10^{-3} M while the sodium (Na^+) concentration decreases from 145 10^{-3} M to 139 10^{-3} M[9]. Therefore, a multiscale approach able to detect the ion concentrations equilibria as well as their deviation from equilibrium conditions is very relevant in biological applications. This would be an invaluable tool for the study and diagnosis of pathological states in biological systems and, more in general, for several emerging fields including environmental monitoring, water control and test, healthcare, agriculture, food, and drink industries.

So far, ion detection and monitoring have been widely addressed with several transistor-based technologies, comprising silicon, zinc-oxide, and graphene ion-sensitive field-effect transistors[10–13], porous silicon extended-gate FETs[14], amorphous indium-gallium-zinc-oxide dual-gate thin-film transistors[15], organic electrolyte-gated FETs[16] and organic electrochemical transistors (OECTs)[17–19]. Among the aforementioned approaches, OECTs are gaining significant interest because they combine superior performance in terms of sensitivity and low-voltage operation, with the typical features of organic technologies, viz. stable operation in aqueous environment, mechanical softness, biological compatibility, ease of integration into arrays, low-cost and large-area fabrication[20–22]. OECTs rely on ionic-electronic charge interaction, which is obtained by putting the electrolyte in direct contact with the electronic channel and the subnanometric ionic-electronic interaction involves the whole microscale volume of the transistor channel[23]. This volumetric response results in an outstanding ion-to-electron transduction.

OECT-based ion sensors[17–19,24] mostly focus on a material or transistor architecture approach, and the resulting sensitivity is defined by the fundamental Nernst limit equal to 59 mV dec^{-1}[25]. This is very far from the ideal sensitivity limit, which can be set to about 1000 mV dec^{-1} assuming the maximum supply voltage for stable operation in aqueous environment, viz. 1 V, and a minimum ion concentration range of one decade. To improve the sensitivity, we recently proposed a current-driven OECT architecture, achieving selective K^+ sensitivity up to 414 10^{-3} V dec^{-1} over an ion concentration range 10^{-2} M $- 1$ M at a supply voltage equal to 0.8 V[26]. However, although sensitive this approach requires a read-out scheme not ideally suitable for real-time ion sensing[27]. Therefore, while OECTs are a promising technology for ion detection and real-time monitoring, current approaches

still require additional electronic circuits for signal amplification because of the limited sensitivity. Even more importantly, the possibility to detect both the ion concentration in a wide range and track small variations of the ion concentration with respect to the detected concentration – viz. multiscale high-sensitivity ion detection – is still an open challenge.

Here we show simultaneous multiscale real-time and high-sensitivity ion detection with complementary OECTs integrated in a push-pull amplifier configuration. The ion sensing amplifier provides both ion-to-electron transduction and signal amplification demonstrating selective real-time ion detection with a sensitivity up to 1172 mV dec^{-1} at a supply voltage equal to 0.5 V and with an operative range of 10^{-5} M–1 M. This results in a voltage sensitivity normalized to the supply voltage larger than 2300 mV V^{-1} dec^{-1}, the highest value ever reported. The high sensitivity allows to monitor variations of the concentration of physiologically relevant ions in human blood serum lower than 20%, making the complementary OECT amplifier a suitable technology for the detection of pathological states through ion sensing. Importantly, we demonstrate that the performances can be enhanced and easily tuned by means of simple design parameters. The high sensitivity combined with the multifunctional reconfiguration enable both ion detection over a range of five orders of magnitude and real-time monitoring of variations two orders of magnitude lower than the detected concentration, viz. multiscale high-sensitivity ion detection.

Results

Ion sensitive OECT complementary amplifier. The ion sensitive OECT amplifier consists of a p-type and an n-type OECT connected in series (Fig. 1a). This circuit configuration is a universal building block used in digital electronic circuits to implement the NOT logic function[28–32]. Here we use this circuit topology following an unexplored OECT-aware analog design approach, where local transduction and amplification are integrated in the same device. Moreover, the use of the complementary configuration results in enhanced gain and reduced power consumption compared with unipolar resistive-based OECT amplifiers used for electrophysiological signal amplification[33,34].

The prototypical conductive polymer poly (3,4-ethylenedioxythiophene) doped with poly(styrene sulfonate) (PEDOT:PSS) is used for the p-type OECT and poly (benzimidazobenzophenanthroline) (BBL) is used for the n-type OECT[32] (details on the fabrication are provided in the "Methods" section). Both polymers show very good stability in aqueous environment, are commercially available, and the corresponding OECTs display comparable ON currents (Supplementary Fig. 1). The polymers show top performing electrical properties among the OECT materials[35], enabling the integration of high performance OECT amplifiers.

A typical transfer characteristic V_O-V_I of the fabricated ion sensitive OECT complementary amplifier is shown in Fig. 1b. The characteristic displays a rail-to-rail output voltage swing with five distinct regions, which correspond to different operating conditions of the p-type and n-type OECTs. More in detail, when $V_I = 0$ V, the n-type OECT is turned off, whereas the p-type OECT is highly conductive and works in the linear regime, resulting in $V_O = V_{DD}$ (Fig. 1b, region 1, $V_I < 0.2$ V). By increasing V_I, the pull-up action of the p-type OECT becomes weaker while the pull-down of the n-type OECT increases and, as a consequence, the output voltage decreases (region 2, 0.2 V < V_I < 0.3 V). Interestingly, when $V_I \approx 0.3$ V the output voltage V_O shows a sharp and large variation (region 3). This transition region is very narrow and extends of only few millivolts around the transition voltage V_M, which we define as the input voltage V_I
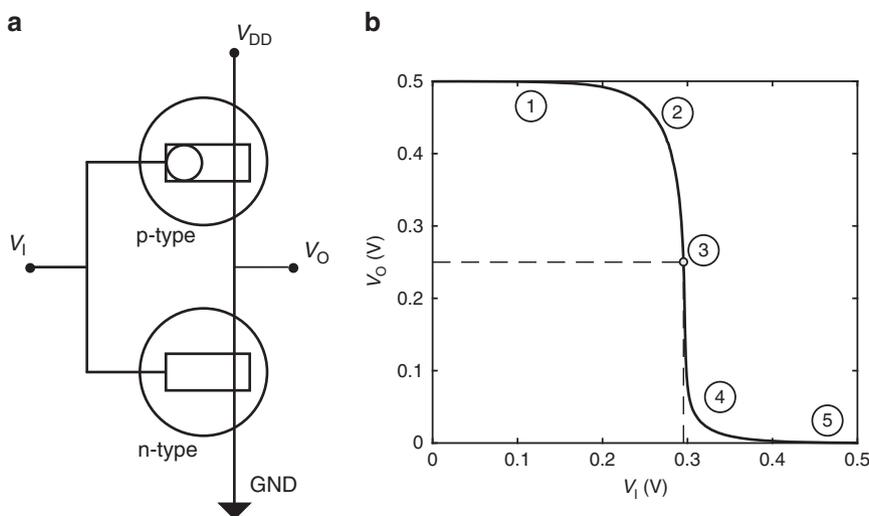
Fig. 1 Organic electrochemical transistor complementary amplifier. a Organic electrochemical transistor complementary amplifier architecture. The input voltage (V_I) is connected to the gates of the transistors, and the output voltage (V_O) is collected at their drains. The supply voltage (V_{DD}) is connected to the source of the p-type OECT, and the source of the n-type is grounded (GND, $V_{GND} = 0$ V). **b** Typical transfer characteristic of an OECT complementary amplifier. The gray dot identifies V_M (viz. the required V_I to have $V_O = V_{DD}/2$) and the various regions of operation are highlighted with numbers.
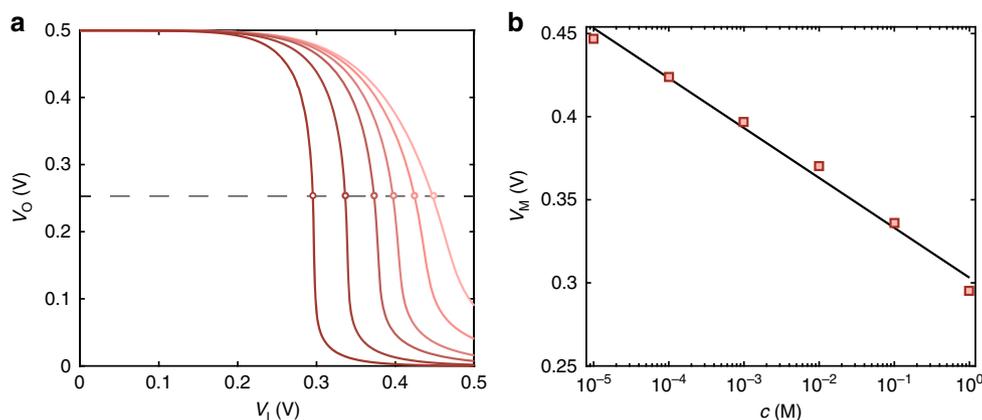

Fig. 2 Wide range operation. a Measured (thick red lines) transfer characteristics of the organic electrochemical transistor complementary amplifier at various ion concentrations. From the rightmost to the leftmost characteristic the ion concentration is equal to [10^{-5}, 10^{-4}, 10^{-3}, 10^{-2}, 10^{-1}, 1] M. **b** Measured V_M as a function of c (square symbols). A sensitivity equal to $S_M = 30$ mV dec^{-1} is obtained with the least square linear approximation (solid line) of the measurements.

required to obtain $V_O = V_{DD}/2$ (gray dot). In other words, close to V_M, small variations of V_I result in large variations of V_O, thus providing a large amplification $A = dV_O/dV_I$. It is worth to note that this amplification is inherently related to the circuit configuration that enables the simultaneous high-gain operation (saturation regime) of both p-type and n-type OECTs. In this regard, OECTs are the ideal technology for this amplifier circuit architecture because they provide both large transconductance g_m[36] and output resistance r_o[37], which eventually result in a large intrinsic gain equal to $g_m r_o$[38]. When V_I is few millivolts larger than V_M, the p-type OECT still operates in the saturation regime while the n-type OECT switches to the linear regime (region 4, 0.3 V $< V_I <$ 0.4 V). By further increasing V_I the output voltage approaches GND (region 5, $V_I >$ 0.4 V).

Wide range ion detection. To investigate the ion response of the OECT-based complementary amplifier, we measured the V_O-V_I characteristics as a function of the ion concertation c in the range 10^{-5} M to 1 M. Figure 2a shows that the measured electrical characteristics (full lines) systematically shift and the transition

voltage V_M (marked with dots in Fig. 2a) reduces by increasing the ion concentration. Figure 2b shows V_M as a function of c. V_M decreases by increasing c with a sensitivity $S_M = \partial V_M / \partial c$ equal to 30 mV dec^{-1} over five orders of magnitude of ion concentration. This can be explained by considering the ion sensitive properties of the OECTs combined with the circuit architecture. More in detail, Lin et al.[25] showed that the measured transfer curves of PEDOT:PSS OECTs shift to more negative gate voltages by increasing the ion concentration. Recently, we demonstrated that this is due to the fixed charges in the polyelectrolyte phase of the polymer, which results in an ion concentration dependent voltage drop at the electrolyte/polyelectrolyte interface and, as a consequence, a threshold voltage shift of the OECT electrical characteristics is measured[39].

The OECT threshold voltage V_T can be related to V_M by considering the OECT complementary amplifier configuration and using the Bernards–Malliaras OECT drain current model[40], V_M reads (see Supplementary Eq. (5), Supplementary Note 1):

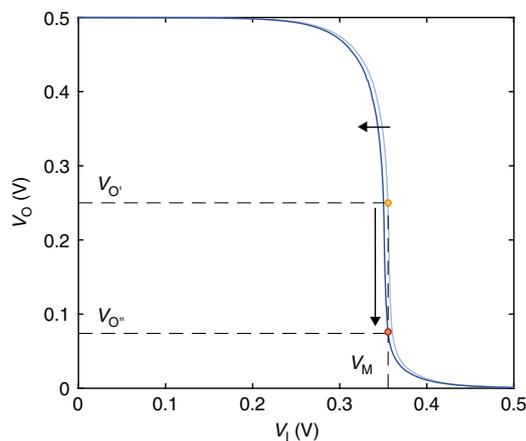$$V_M = \frac{V_{Tn} + \eta V_{Tp} + \eta V_{DD}}{1 + \eta}, \quad (1)$$

Fig. 3 Ionic-to-electronic amplification mechanism. To operate the organic electrochemical transistor complementary amplifier with high sensitivity, the input voltage is biased at $V_I = V_M$, while the output voltage is continuously measured. Light-blue characteristic: at $V_I = V_M$ the output $V_O = V_{O'}$ and the ion concentration is c_0. A small variation of the ion concentration results in a shift of the electrical characteristic (from light-blue to dark-blue) and this, in turn, in a large variation of the output voltage from $V_{O'}$ to $V_{O''}$.

where V_{Tn}, V_{Tp} are the threshold voltages of the p- and n-type OECTs[39], respectively, $\eta = (\Gamma_p \Gamma_n^{-1})^{1/2}$, and Γ_p, Γ_n are the current pre-factors of the p- and n-type OECTs, respectively. Equation (1) shows that V_M depends on the OECTs threshold voltages V_{Tn}, V_{Tp}, and on the designed OECT geometries (viz. Γ_p and Γ_n). Basing on Eq. (1) the sensitivity S_M can be calculated:

$$S_M = \frac{\partial V_M}{\partial c} = \frac{\eta}{1 + \eta} \frac{\partial V_{Tp}}{\partial c}, \qquad (2)$$

where in the case of PEDOT:PSS OETCs $\partial V_{Tp}/\partial c = 59$ mV dec^{-1}[39]. We designed the OECTs in order to have comparable currents, resulting in $\eta \approx 1$ and hence $S_M = 0.5\ \partial V_{Tp}/\partial c$. We note that the ion sensitivity of V_M is smaller than the OECT threshold voltage sensitivity. As a consequence, V_M obtained from the transfer characteristics V_O-V_I enables ion detection in a wide range (10^{-5} M – 1 M) with a supply voltage as low as $V_{DD} = 0.5$ V.

Local ion-to-voltage amplification. Upon ion detection in a wide range, the OECT complementary amplifier is used to detect small variations of the ion concentration with high sensitivity. The previously recorded V_M yields the corresponding ion concentration c_0 according to the calibration curve showed in Fig. 2b. The input voltage V_I is biased at $V_I = V_M$ and in this operating condition, owing to the amplification A of the OECT complementary amplifier configuration, a very small variation of ion concentration results in a large variation of the output voltage V_O. As an example, Fig. 3 shows that V_O varies from $V_{O'} = 0.25$ V (orange dot) to $V_{O''} = 0.08$ V (red dot) in the case the ion concentration variation $\Delta c = c - c_0 = 50\ 10^{-3}$ M and $c_0 = 10^{-1}$ M. More in detail, the output voltage decreases when c increases with respect to the initial concentration c_0, while a larger V_O is displayed when the ion concentration gets lower. The output voltage variation ∂V_O resulting from a concentration variation ∂c can be quantified as follows:

$$S_A = \frac{\partial V_O}{\partial c} = A S_M, \qquad (3)$$

where S_M is given by Eq. (2) and A can be calculated by differentiating the OECT current equation (see Supplementary Eq.

(10), Supplementary note 1) with respect to V_I and results:

$$A(V_M) = \frac{1}{I_D(V_M)} \frac{g_{mn}\left[1 + \lambda_n \frac{V_{DD}}{2}\right] + g_{mp}\left[1 + \lambda_p \frac{V_{DD}}{2}\right]}{\lambda_n + \lambda_p}, \qquad (4)$$

where $I_D(V_M)$ is the current flowing through the OECTs at $V_I = V_M$ and λ_n, λ_p account for the channel length modulation[41] in the n-type and p-type OECTs, respectively. Interestingly, Eq. (4) shows that the OECT complementary amplifier leverages on the combined large transconductance (viz. large g_{mn}, g_{mp}) and output resistance (viz. small $\lambda \propto g_o$, $g_o = r_o^{-1}$) of OECTs to provide, at the same time, enhanced ion-to-voltage transduction and amplification, namely high-sensitivity ion detection. Indeed, OECTs show extremely high g_m[36] and r_o[37] owing to the volumetric ionic-electronic charge interaction, making them ideal components for the fabrication of high-performance ion sensitive amplifiers.

Real-time high-sensitivity operation. The real-time, high-sensitivity monitoring of the ion concentration is shown in Fig. 4a. The input voltage of the OECT complementary amplifier is biased at $V_I = V_M$ and the output voltage V_O is measured over the time while the analyte ion concentration is varied from $54\ 10^{-5}$ M to $1.27\ 10^{-3}$ M. It is worth to note that a variation of c as small as $7\ 10^{-5}$ M, from $54\ 10^{-5}$ to $61\ 10^{-5}$, results in an output voltage response $\Delta V_O = 20$ mV with a response time of only 11 s (Supplementary Fig. 2). Interestingly, such variation is detected with respect to a background concentration of about one order of magnitude larger ($c_0 = 54\ 10^{-5}$). Figure 4b shows the measured steady-state output voltage as a function of c. The least square linear approximation of the measured V_O provides an average sensitivity equal to 640 mV dec^{-1} (Fig. 4b).

The high sensitivity characteristics of the OECT complementary amplifier for various ranges of ion concentrations are displayed in Fig. 4c. We obtained an average voltage sensitivity equal to 640 mV dec^{-1}, 837 mV dec^{-1}, 913 mV dec^{-1}, and 1124 mV dec^{-1}, when c is in the range $5\ 10^{-4}$–10^{-3} M, $5\ 10^{-3}$–10^{-2} M, $5\ 10^{-2}$–10^{-1} M and $5\ 10^{-1}$–10^0 M, respectively. To easily compare the various ion-to-voltage responses of the OECT complementary amplifier, the variation of the output voltage ΔV_O as a function of c normalized to the minimum concentration of the assessed range (viz. c/c_{min}) is displayed in Fig. 4d. At a supply voltage $V_{DD} = 0.5$ V the maximum ΔV_O is about 0.2 V in the lowest range of concentration and it increases to almost 0.3 V in the highest range of concentration. This confirms that the voltage sensitivity increases by increasing the ion concentration range, and this can be explained by considering that the amplification parameter A increases with increasing c (see Supplementary Note 2 and Supplementary Fig. 3). This is an important feature to detect small variations of c even when operating at large equilibrium or background concentrations. More in detail, the minimum ion variation that can be detected is $\Delta c_{min} = [10^{\wedge}(\Delta V_{O,min} S_A^{-1}) - 1] c_{max}$ (see Supplementary Note 2), where c_{max} is the maximum concentration in the operative range, S_A is the sensitivity and ΔV_{Omin} is the corresponding minimum output voltage variation. To be conservative, we assume $\Delta V_{Omin} = 1\%\ V_{DD}$, viz. in our case $\Delta V_{Omin} = 5\ 10^{-3}$ V, and this gives $\Delta c_{min} = 1.8\ 10^{-5}$ M, $1.4\ 10^{-4}$ M, $1.3\ 10^{-3}$ M, $1.0\ 10^{-2}$ M when $c_{max} = 10^{-3}$ M, 10^{-2} M, 10^{-1} M, 10^0 M, respectively. Therefore, the OECT complementary amplifier provides $\Delta c_{min}\ /\ c_{max} \cong 1\%$ over the whole assessed range (viz. $5\ 10^{-4}$–10^0 M). This performance perfectly fits the most challenging physiological applications that require the detection of ion variations of the order of 10^{-3} M when the ion concentration is in the range $10\ 10^{-3}$–$100\ 10^{-3}$ M[7–9].

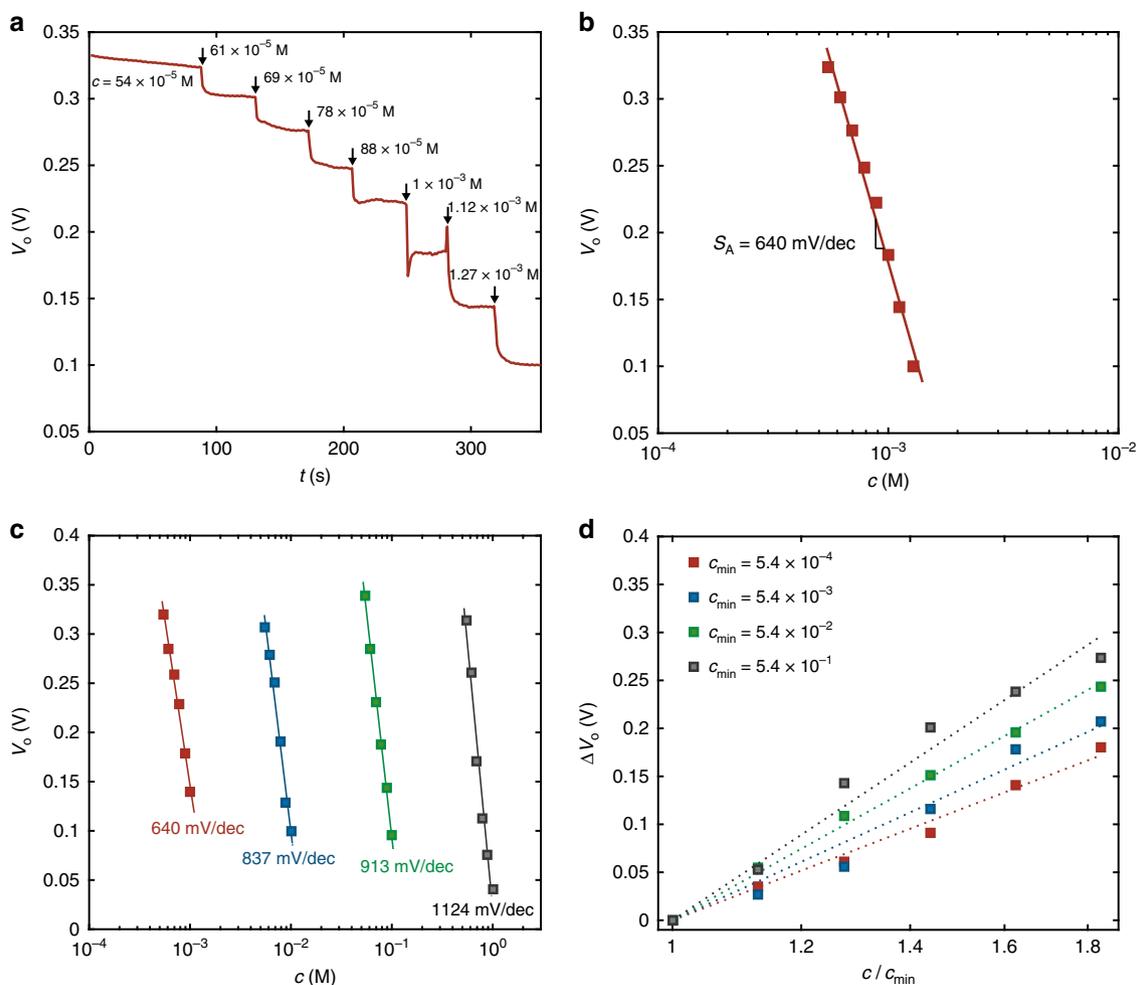**Fig. 4 Real time high sensitivity operation. a** Real time high-sensitivity ion detection in the concentration range 54×10^{-5} M – 1.27×10^{-3} M. The electrolyte concentration is increased every 30 s. The measurements are performed at $V_M = 0.415$ V. **b** Measured steady-state output voltage V_O (symbols) as a function of ion concentration c. Full red line is the linear least square fit to the measurements and yields a sensitivity $S_A = 640$ mV dec^{-1}. **c** Measured V_O as a function of c in various sub-range of concentrations, covering the whole physiological range. The ion concentration where $V_O = V_{DD}$ / 2 is $c_0 = [7.8 \times 10^{-4}, 7.8 \times 10^{-3}, 7.8 \times 10^{-2}, 7.8 \times 10^{-1}]$ M. Full lines are the linear least square fit to the measurements, yielding S_A. **d** Measured (symbols) output voltage variation $\Delta V_O = V_O(c) - V_O(c_{min})$ as a function of c / c_{min}, where $c_{min} = [5.4 \times 10^{-4}, 5.4 \times 10^{-3}, 5.4 \times 10^{-2}, 5.4 \times 10^{-1}]$ M. Dotted lines are guides for the eye.

Tuning of the ion sensitive performances. In contrast to single transistor approaches where the performances are imposed by the device physics, the proposed circuit-oriented approach allows to tune the ion sensing performances by design of the circuit parameters. Importantly, the understanding of the OECT amplifier provided in the previous sections gives precise information on the design parameters in order to tailor the target figures of merit and performance. As a relevant example, here we show that the sensitivity of the OECT complementary amplifier can be easily tuned to meet specific requirements of various application fields, which is important to broad its use. According to Eq. (4), the ion sensitivity depends on both technological and circuit parameters (g_{mn}, g_{mp}, λ_n, λ_p) and on the supply voltage V_{DD}. Therefore, the design of the OECTs parameters allows to set the ion detection performances at the fabrication stage, while the dependence of the sensitivity on V_{DD} enables dynamic electrically-reconfigurable ion sensing response. Figure 5 displays the output voltage variation as a function of c/c_{min} when the OECT amplifier is operated at several V_{DD}. The required sensitivity and subrange of ion concentration can be finely tuned by simply changing V_{DD}. More in detail, when $c_{min} = 5$ 10^{-2}, a supply voltage of 0.5 V allows to detect concentration variations

with a sensitivity of 913 mV dec^{-1} up to $c = 1.8$ c_{min} (dark green squares). By lowering the V_{DD} to 0.4 V the sensitivity reduces to 483 mV dec^{-1}, extending the sub-range to $c = 2.8$ c_{min} (green circles), while at $V_{DD} = 0.3$ V the sensitivity is equal to 267 mV dec^{-1} up to $c = 3.8$ c_{min} (light green triangles).

Multiscale ion-selective operation. Ion selectivity using the OECT complementary amplifier is obtained by integrating ion selective membranes (ISMs). Analogously to the ion-selective sensors based on organic transistors[16,17,19], ISM is placed between the gate and the channel. The ISMs are fabricated according to the methods reported in Ref. [17] (see "Methods" section). As a relevant application, we show K$^+$-selective OECT complementary amplifiers. K$^+$ plays a fundamental role in human body, being involved in the regulation of intracellular water uptake, in the transmission of neural signals and in muscles contraction[1]. The electrical characteristics of the K$^+$-selective OECT complementary amplifier are measured as a function of the K$^+$ concentration c^{K+}. Figure 6a displays V_M as a function c^{K+} in the range from 10^{-5} to 1 M. It shows that V_M decreases with increasing c^{K+} in agreement with the measurements without the K$^+$-selective membrane (Fig. 2b).
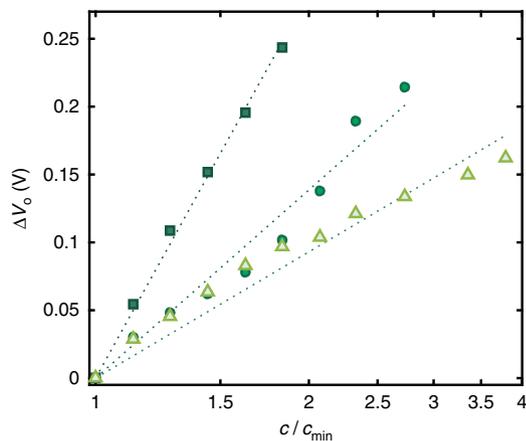
Fig. 5 Tuning of the amplifier sensitivity. Measured (symbols) output voltage variation $\Delta V_O = V_O(c) - V_O(c_{min})$ by varying the operating voltage V_{DD}. The dark green squares are measured at $V_{DD} = 0.5$ V and c equal to [5.4, 6.1, 6.9, 7.8, 8.8, 10] x 10^{-2} M, the green circles are measured at $V_{DD} = 0.4$ V and c equal to [5.4, 6.1, 6.9, 7.8, 8.8, 10, 11.3, 12.7, 14.9, 18.3] x 10^{-2} M and the light green triangles are measured at $V_{DD} = 0.3$ V and c equal to [5.4, 6.1, 6.9, 7.8, 8.8, 10, 11.3, 12.7, 14.9, 18.3, 20.6] x 10^{-2} M. Dotted lines are guides for the eye.

Upon selective K^+ detection over wide range, the input voltage of the OECT complementary amplifier is biased at $V_I = V_M(K^+)$ and V_O is measured as a function of time by varying the K^+ concertation into the analyte solution. Figure 6b shows that the measured V_O decreases with increasing K^+ concentration and the linear least square approximation of the measured V_O as a function of K^+ provides an average sensitivity equal to 703 mV dec^{-1}, 952 mV dec^{-1}, 995 mV dec^{-1}, and 1172 mV dec^{-1}, when K^+ is in the range $5 \cdot 10^{-4}$–10^{-3} M, $5 \cdot 10^{-3}$–10^{-2} M, $5 \cdot 10^{-2}$–10^{-1} M, and $5 \cdot 10^{-1}$–10^{0} M, respectively. It is worth to note that the measured sensitivity is in full agreement with the sensitivity obtained without the ion selective membrane (Fig. 4c) demonstrating that the use of ISM does not reduce the OECT amplifier sensitivity.

The selectivity of the ion selective OECT amplifier against other physiologically relevant ions is displayed in Fig. 6c–f. In Fig. 6c the K^+ concentration is constant and amounts to $5.4 \cdot 10^{-2}$ M, while the Na^+ concentration is systematically increased from $5.4 \cdot 10^{-2}$ M to $1 \cdot 10^{-1}$ M. The measured output voltage V_O as function of time is independent of the Na^+ spiked to the electrolyte solution, as confirmed by Fig. 6d where the measured steady state V_O is displayed as a function of the Na^+ concentration. A negligible response is triggered by the Na^+ concentration and the cross-sensitivity amounts to 33 mV dec^{-1}, which is about 30-folds lower than the K^+ sensitivity in the same range of concentrations (i.e., 995 mV dec^{-1}) and 20-folds lower than the minimum K^+ sensitivity (i.e., 703 mV dec^{-1} in the range $5 \cdot 10^{-4} - 1 \cdot 10^{-3}$ M) (Supplementary Fig. 4). As a further confirmation, we assessed the selectivity against Ca^{2+}, a relevant bivalent ion present in physiological systems. The Ca^{2+} concentration is systematically increased from $5.4 \cdot 10^{-2}$ M to $1 \cdot 10^{-1}$ M and, as showed in Fig. 6e, the measured V_O as function of time is independent of the Ca^{2+} spiked to the electrolyte solution. Figure 6f shows the measured steady state V_O as a function of the Ca^{2+} concentration. A negligible response is triggered by the Ca^{2+} concentration and the cross-sensitivity amounts to 20 mV dec^{-1}, which is about 50-folds lower than the K^+ sensitivity in the same range of concentrations (i.e., 995 mV dec^{-1}) and 35-fold lower than the minimum K^+ sensitivity (i.e., 703 mV dec^{-1} in the range $5 \cdot 10^{-4}$–$1 \cdot 10^{-3}$ M) (Supplementary Fig. 4). Therefore, we can conclude that the

ion selective OECT complementary amplifier architecture dramatically enhances the sensitivity of ISM-based OECT ion sensors while ensuring selective response.

Blood serum ion monitoring. As practical and feasible application of the complementary OECT amplifier in the biomedical field, high-sensitivity and selective ion detection in blood serum is demonstrated. Figure 7a shows the real-time monitoring of potassium in blood serum with the complementary OECT amplifier. The input voltage is biased at 0.37 V and the output voltage is continuously measured over time. The analyte is human blood serum, with a starting potassium concentration of 4.8 10^{-3} M and a background sodium concentration of 1.36 10^{-1} M, i.e., about 2 orders of magnitude larger than the K^+ concentration. The output voltage is continuously measured over time by varying the potassium concentration from 4.8 10^{-3} M to 9.6 10^{-3} M, which are K^+ concentrations representative of heathy and pathological states. We note that the K^+ concentration of the blood serum is varied by spiking the analyte with a small amount of 1 10^{-1} M KCl solution. Figure 7a shows that when the analyte K^+ concentration is increased, the output voltage readily and systematically decreases. The measured steady state V_O as a function of c is shown in Fig. 7b. The least square linear approximation of the V_O-c characteristic yields an average sensitivity equal to 662 mV dec^{-1}, which is in agreement with that obtained in the case of KCl water solution in the same range of c. The selectivity control experiment is displayed in Fig. 7c, where the starting sodium concentration of 1.36 10^{-1} M is increased over time reaching up to 2.72 10^{-1} M by spiking with a 5 M NaCl solution. A negligible variation of the measured output voltage is displayed. We note that the maximum Na^+ concentration assessed in this experiment is larger than the maximum value reached in humans' blood[42]. Figure 7d shows the measured steady state output voltage as a function of the Na^+ concentration, showing a cross-sensitivity of 44 mV dec^{-1}. The comparison between the OECT amplifier response in terms of ΔV_O vs. c/c_{min} is displayed in Supplementary Fig. 5, demonstrating that a twofold variation in the K^+ concentration yields $\Delta V_O = 190$ mV, while the same Na^+ variation results in $\Delta V_O = 15$ mV. Importantly, the complementary OECT amplifier is able to sense a deviation of the K^+ concentration lower than the 20%, yielding an output variation of 45 mV when the concentration increases from 4.8 10^{-3} M to 5.7 10^{-3} M.

Benchmarking transistor-based ion sensors. To fairly compare the sensing performance of the OECT complementary amplifier with various transistor-based ion sensor technology platforms, we calculated the sensitivity normalized to the supply voltage $S_N = S_A V_{DD}^{-1}$. Figure 8a shows the sensitivity enhancement obtained by the OECT complementary amplifier with respect to the theoretical limit, which is given by the maximum sensitivity of a sensor normalized to the minimum supply voltage required to access the target range of concentration. Therefore, when the concentration range is equal to five orders of magnitude the theoretical limit results 200 10^{-3} V V^{-1} dec^{-1}. Interestingly, the maximum S_N obtained by the proposed architecture is 2344 mV V^{-1} dec^{-1}, more than one order of magnitude larger than the theoretical limit of transistor-based ion sensors.

In Fig. 8b the sensitivity and operating range of the ion selective OECT complementary amplifier is benchmarked against various transistor-based ion sensors devices and architectures, including silicon[10,12], porous-Si[14], graphene[11], zinc-oxide[13], amorphous In-Ga-ZnO[15], and organic materials technologies[16–19,43]. It shows that state-of-the-art ion sensors provide either wide operating range with small S_N, or average S_N over a narrow range. Owing to the
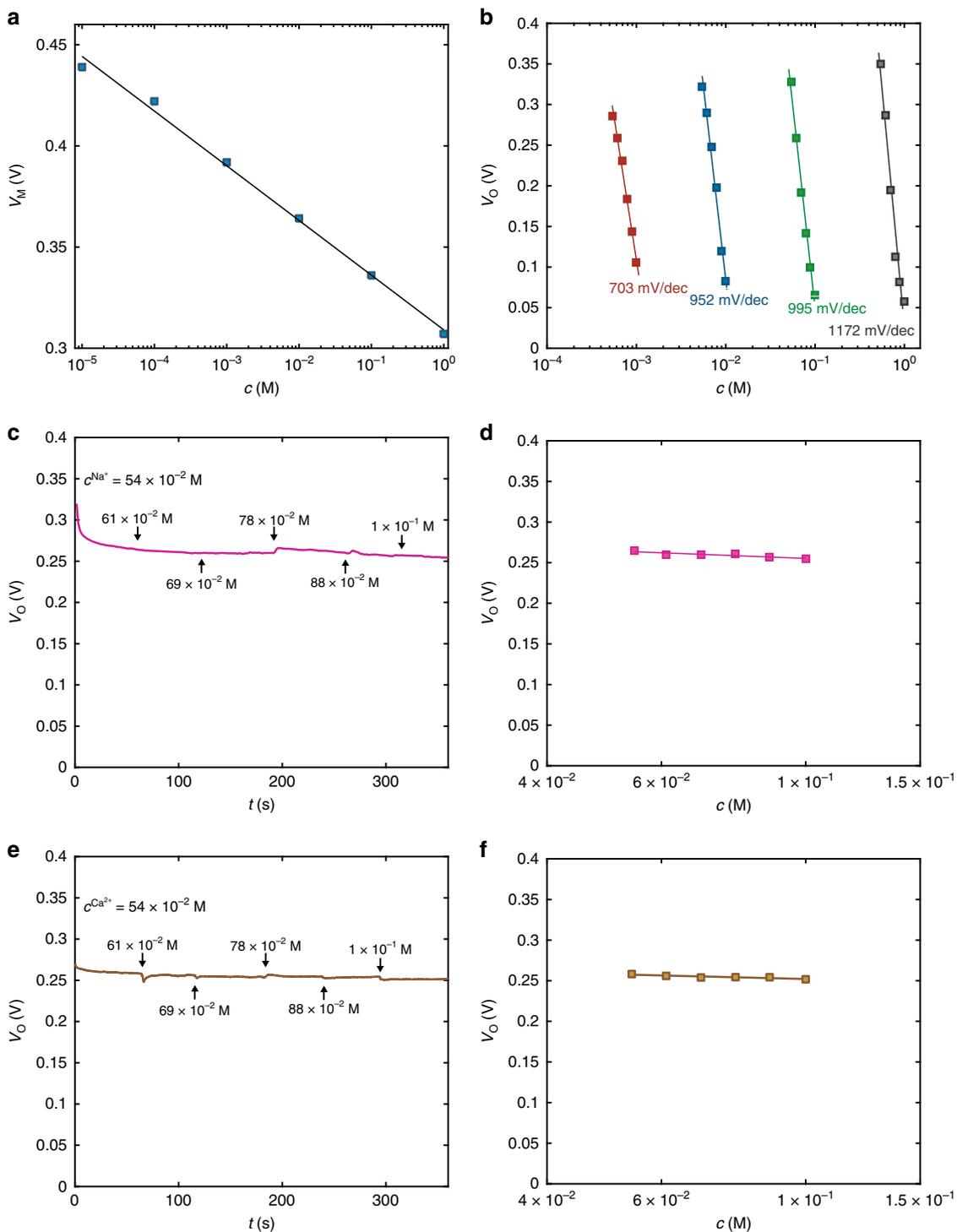
Fig. 6 Selective ion detection and real time monitoring. a Measured (symbols) V_M as a function of the potassium concentration for the potassium selective organic electrochemical transistor complementary amplifier. The full line is the linear least square fit to the measurements, and its slope gives a wide-range sensitivity $S_M = 28$ mV dec^{-1}. **b** Measured (symbols) V_O – c^{K+} high sensitivity characteristics comprising the whole physiological range. Solid lines are the linear least square fit to the measurements, yielding $S_A = 703$ mV dec^{-1}, 952 mV dec^{-1}, 995 mV dec^{-1}, 1172 mV dec^{-1}. **c, e** Control experiment demonstrating the selectivity of the potassium-selective OECT complementary amplifier. V_O is measured over time and the Na$^+$ (**c**) or Ca^{2+} (**e**) concentration is systematically increased every 60 s from 5.4 10^{-2} M to 1 10^{-1} M. In both cases the K$^+$ concentration is constant and amounts to 5.4 10^{-2} M. **d, f** Measured (symbols) steady state V_O as a function of c^{Na+} (**d**) or c^{Ca2+} (**f**). Solid line is the linear least square fit to the measurements and yields a cross-sensitivity $S_{CR,Na+} = 33$ mV dec^{-1} for Na$^+$, and $S_{CR,Ca2+} = 20$ mV dec^{-1} for Ca^{2+}, confirming the excellent selectivity of the output response.
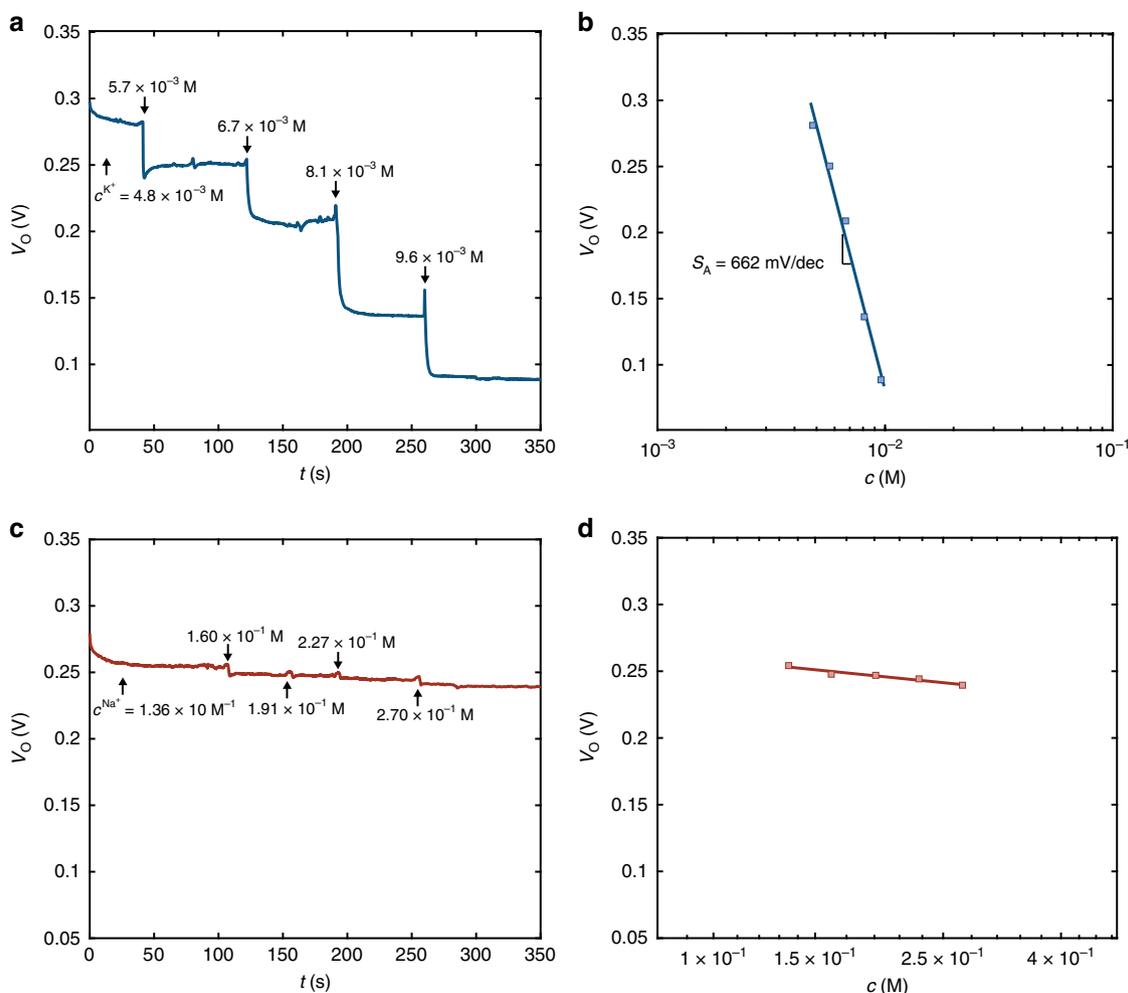
Fig. 7 Selective K^+ sensing in human blood serum. a Real time high sensitivity K^+ detection in human blood serum. The K^+ concentration range is $4.8\,10^{-3}$ M – $9.6\,10^{-3}$ M. The potassium concentration of the blood serum is increased over time by spiking small amounts of $1\,10^{-1}$ M KCl water solution. The measurements are performed at $V_I = 0.37$ V. **b** Measured steady-state output voltage V_O (symbols) as a function of K^+ concentration c. Full blue line is the linear least square fit to the measurements and yields a sensitivity $S_A = 662$ mV dec^{-1}. **c** Control experiment demonstrating the selectivity against sodium in blood serum. V_O is measured over time and the Na^+ concentration of the blood serum is systematically increased from $1.36\,10^{-1}$ M to $2.70\,10^{-1}$ M. The K^+ concentration is constant and amounts to $4.8\,10^{-3}$ M. **f** Measured (symbols) steady state V_O as a function of c^{Na+}. Solid line is the linear least square fit to the measurements and yields a cross-sensitivity equal to 44 mV dec^{-1}, which is more than 15-fold lower than the sensitivity of the selected K^+ ions.

circuit-oriented multiscale approach, the OECT complementary amplifier device yields both superior sensitivity and wide range, providing easily-tunable ion-to-electron local transconduction and amplification. The performances are compared with more detail in Table 1. In addition to the multiscale high-sensitivity operation, the proposed OECT amplifier provides real time sensing capabilities and the supply voltage is amongst the lowest reported. As a result, the complementary OECT amplifier is able to selectively detect in real-time a variation of the K^+ concentration lower than 20% from the normal resting conditions, meeting the requirements for hypo- and hyperkalemia detection in blood serum[8].

Discussion
Prospectively, the OECT complementary amplifier approach could be extended to a wide range of transistor-based bioelectronic technologies including for example, immunosensors[44] as well as metabolites[45–48], hormones[49], DNA[50], peptides[51], proteins[52] and viruses[53,54], detection. Along this direction, an emerging and rapidly growing research field is the single molecule detection with millimeter-sized transistors[55–59] where the biorecognition events result in a shift of the transistor threshold

voltage, which is typically of the order of few millivolts. The high-sensitivity, multiscale and reconfigurable operation provided by the OECT complementary amplifier can be extremely relevant also in this emerging research field to improve the signal-to-noise ratio, resolution and robustness, eventually achieving ultimately sensitive enhanced bioelectronics[60,61].

In conclusion, the proposed multiscale approach is a simple and effective way to capture the whole problem complexity without overlooking the smallest but meaningful details. Just like when we look at a big painting, first we have a global look at the context, then we get closer to appreciate a tiny detail, a hidden message or the brushstroke (Supplementary Fig. 6). In the same way, the ion sensitive OECT complementary amplifier provides ion sensing over wide range, i.e., the panoramic view of the problem, and high sensitivity detection, allowing to capture the tiny ion concentration variations that could be the meaningful fingerprint of pathological onsets. The top performing range and the unprecedented sensitivity, combined with real-time operation, tunable performances and low operating supply voltage, are enabled by a circuit-oriented device-aware sensor design approach. The proposed approach is general, and it can be extended to other sensing applications and transistor
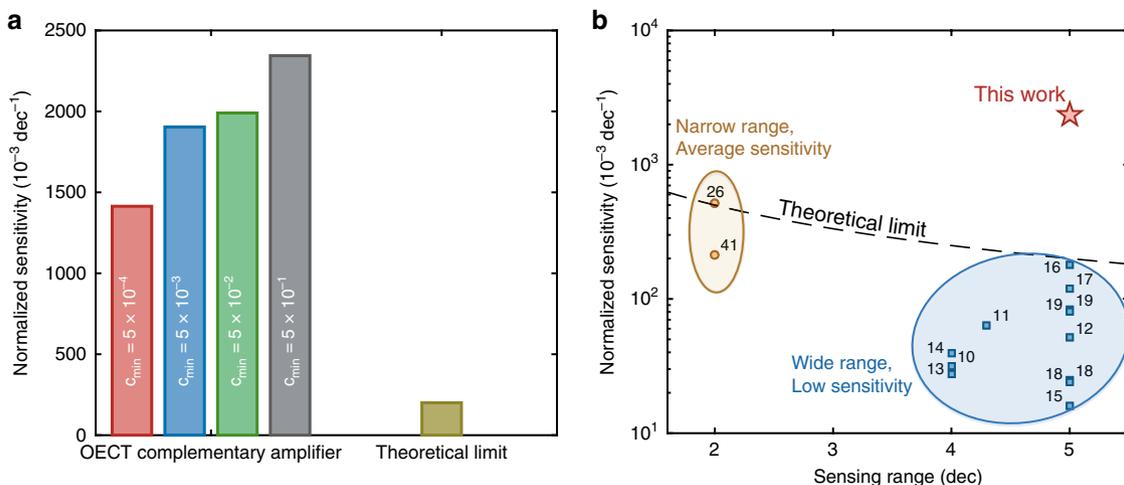
Fig. 8 Sensing performance benchmark. a Normalized Sensitivity S_N of the organic electrochemical transistor complementary amplifier compared with the theoretical limit for ion detection over 5 orders of magnitude. The S_N for the complementary OECT amplifier is equal to [1414,1904,1990,2344] mV V^{-1} dec^{-1} when c_{min} is equal to [5.4×10^{-4} 5.4×10^{-3} 5.4×10^{-2} 5.4×10^{-1}] M, respectively, while the theoretical fundamental limit is equal to 200 mV V^{-1} dec^{-1}. **b** Comparison between the normalized sensitivity and sensing range of the proposed OECT complementary amplifier with state-of-the-art ion sensors. It is worth to note that the S_N is obtained as mV^{-1} V^{-1} dec^{-1} when the output of the ion sensor is expressed as a voltage, while it is obtained as μA^{-1} mA^{-1} V when the output is a current. In both cases it yields 10^{-3} dec^{-1}.

Table 1 Sensing performances comparison.

Technology	Material	Selected ion	Supply voltage [V]	Ion concentration range [dec]	Normalized Sensitivity		Real-time ion detection	Ref.
					Current [μA mA⁻¹ dec⁻¹]	Voltage [mV V⁻¹ dec⁻¹]		
ISFET	Silicon	Na+, K+	1.8	4	–	31.6	✓	10
ISFET	Graphene	K+	1.0	4.3	–	64.0	✓	11
Hybrid ISFET	Silicon	K+	2.0	5	–	52.0	✓	12
Single-gate TFT	ZnO	pH	2.0	4	–	27.5	–	13
double-gate TFT	a-IGZO	pH	10.0	5	–	16.0	–	15
Extended-gate FET	Porous-Si	Na+, K+	1.5	4	11	39.2	–	14
EGOFET	P3HT	Na+	0.5	5	179	124.0	✓	16
OECT	PEDOT:PSS	K+	0.4	5	72	120.0	✓	17
Current-driven OECT	PEDOT:PSS	K+	0.8	2	–	517.5	–	26
Current-driven OECT	IL-doped PEDOT:PSS	Na+	0.7	2	–	214.3	–	42
Integrated IS-OECT	PEDOT:PSS	Na+	0.6	5	–	83.3	–	19
Integrated IS-OECT	PEDOT:PSS	K+	0.6	5	–	80.0	–	19
Membraneless OECT	p(T15c5-ran-EDOT) / PEDOT:PSS	Na+	1.2	5	25	–	✓	18
Membraneless OECT	p(T18c6-ran-EDOT) / PEDOT:PSS	K+	1.2	4	24	–	✓	18
OECT complementary amplifier	PEDOT:PSS, BBL	K+	0.5	5	–	2344.0	✓	This work

The table compares the performances of several transistor-based sensor technologies by considering the type of ion, the supply voltage (V_{DD}), the sensing range, the normalized sensitivity S_N and the real-time detection capability.

technologies, paving the way to enhanced multifunctional ion detection and opening opportunities for high-performance bioelectronics.

Methods

Device fabrication. OECTs were fabricated following the procedure described in Ref. [62]. Briefly, gold source and drain electrodes were deposited by sputtering, using chromium as adhesion layer, on a 26×76 mm² glass slide. The electrodes were photolithographically patterned, defining the channels dimensions. The p-type

channel width (W) and length (L) are 200 μm and 50 μm, respectively. The n-type devices interdigitated electrodes defined $W = 80$ mm, $L = 20$ μm. A first layer of parylene-C is deposited to isolate the contact lines from the electrolyte, and a second sacrificial layer is deposited on top of it to enable polymer patterning with a peel-off procedure. Soap is used to separate the two parylene-C layers, enabling the peel-off of the sacrificial layer. PEDOT:PSS (Clevios PH 1000) was mixed with 5% ethylene glycol, 0.1 wt% dodecyl benzene sulf acid and 1 wt% of (3-glycidylox-ypropyl) trimethoxysilane, and spin coated at 1000 rpm for 60 s. The devices were baked at 140 °C for 1 h. BBL was mixed with Methanesulfonic Acid (5 mg/ml) and stirred overnight at 70 °C. The obtained solution was spin coated at 400 rpm for

60 s, then the glass slide was soaked in DI water for 1 h. The devices were baked at 140 °C for 4 h.

Ion selective membranes fabrication. High molecular weight PVC (36.5 wt.%) was mixed with potassium ionophore III (2.5 wt.%), potassium tetrakis(4-chlor-ophenyl-)borate (0.5 wt.%) and diisodecyl adipate (60.5 wt.%) in tetrahydrofuran THF (500 mg/5 mL). The mixture was spin coated at 300 rpm for 120 s. A rubber ring defined the membrane dimension and provided mechanical stability. ISM-OECT: a PDMS well was used to confine the filling solution (1 M NaCl) and provided mechanical support to the membrane. A small well is placed on top of the stack to confine the analyte.

Electrical characterization. The measurements were performed using KCl or NaCl at several concentrations. Human blood serum was purchased from Sigma-Aldrich and used as received, with a starting KCl concentration of 5×10^{-3} M. A tin wire was used for PEDOT:PSS OECT gate electrode, while Ag/AgCl was used for the BBL OECT gate. The electrical characteristics were measured with two Keithley 2636 A. Ad-hoc microfluidics are designed to provide electrical connection to the device and a housing for the analyte (See Supplementary Fig. 7). The OECT complementary amplifier transfer characteristics were measured by sweeping the input voltage from 0 V to V_{DD} with a rate of 10 mV/s.

Data availability
The data that support the findings of this study are available from the corresponding author on reasonable request.

References
1. Vander, A., Sherman, J. & Luciano, D. *Human Physiology: The Mechanisms of Body Function*. 8th edn (McGraw-Hill, New York, 2001).
2. Nieves-Cordones M., Al Shiblawi F.R., Sentenac H. (2016) Roles and Transport of Sodium and Potassium in Plants. In: Sigel A., Sigel H., Sigel R. (eds) The Alkali Metal Ions: Their Role for Life. Metal Ions in Life Sciences, vol 16. Springer, Cham.
3. Pardo, J. M. & Quintero, F. J. Plants and sodium ions: keeping company with the enemy. *Genome Biol.* 3, 1017.1–1017.4 (2002).
4. Maas, E. V., Plant growth response to salt stress. In: Lieth, H. & Al Masoom, A. A. (eds) Towards the rational use of high salinity tolerant plants. Tasks for vegetation science, vol 27. Springer, Dordrecht.
5. Jentsch, T. J., Hübner, C. A. & Fuhrmann, J. C. Ion channels: function unravelled by dysfunction. *Nat. Cell Biol.* 6, 1039–1047 (2004).
6. He, F. J. & MacGregor, G. A. A comprehensive review on salt and health and current experience of worldwide salt reduction programmes. *J. Hum. Hypertens.* 23, 363–384 (2009).
7. Cozzolino, O. et al. Understanding spreading depression from headache to sudden unexpected death. *Front. Neurol.* 9, 19 (2018).
8. Rastegar, A. Serum potassium. In: Walker, H. K., Hall, W. D. & Hurst, J. W. (Eds.). Clinical methods: the history, physical, and laboratory examinations. 3rd ed. (Boston, MA: Butterworths; 1990).
9. Raimondo, J. V., Burman, R. J., Katz, A. A. & Akerman, C. J. Ion dynamics during seizures. *Front. Cell. Neurosci.* 9, 419 (2015).
10. Zhang, J. et al. Sweat biomarker sensor incorporating picowatt, three-dimensional extended metal gate ion sensitive field effect transistors. *ACS Sens* 4, 2039–2047 (2019).
11. Li, H. et al. Graphene field effect transistors for highly sensitive and selective detection of K^+ ions. *Sens. Actuators B Chem.* 253, 759–765 (2017).
12. Bao, C., Kaur, M. & Kim, W. S. Toward a highly selective artificial saliva sensor using printed hybrid field effect transistors. *Sens Actuators B Chem.* 285, 186–192 (2019).
13. Yano, M. et al. Zinc oxide ion-sensitive field-effect transistors and biosensors. *Phys. Status Solidi Appl. Mater. Sci.* 211, 2098–2104 (2014).
14. Kabaa, E. A., Abdulateef, S. A., Ahmed, N. M., Hassan, Z. & Sabah, F. A. A novel porous silicon multi-ions selective electrode based extended gate field effect transistor for sodium, potassium, calcium, and magnesium sensor. *Appl. Phys. A* 125, 753 (2019).
15. Kumar, N., Kumar, J. & Panda, S. Back-channel electrolyte-gated a-IGZO dual-gate thin-film transistor for enhancement of pH sensitivity over nernst limit. *IEEE Electron Device Lett.* 37, 500–503 (2016).
16. Schmoltner, K., Kofler, J., Klug, A. & List-Kratochvil, E. J. W. Electrolyte-gated organic field-effect transistor for selective reversible ion detection. *Adv. Mater.* 25, 6895–6899 (2013).
17. Sessolo, M., Rivnay, J., Bandiello, E., Malliaras, G. G. & Bolink, H. J. Ion-selective organic electrochemical transistors. *Adv. Mater.* 26, 4803–4807 (2014).
18. Wustoni, S. et al. Membrane-Free Detection of Metal Cations with an Organic Electrochemical Transistor. *Adv. Funct. Mater.* 29, 1904403 (2019).
19. Pierre, A., Doris, S. E., Lujan, R. & Street, R. A. Monolithic integration of ion-selective organic electrochemical transistors with thin film transistors on flexible substrates. *Adv. Mater. Technol.* 4, 1800577 (2019).
20. Rivnay, J. et al. Organic electrochemical transistors. *Nat. Rev. Mater.* 3, 17086 (2018).
21. Rivnay, J., Owens, R. M. & Malliaras, G. G. The rise of organic bioelectronics. *Chem. Mater.* 26, 679–685 (2014).
22. Zeglio, E. & Inganäs, O. Active materials for organic electrochemical transistors. *Adv. Mater.* 30, 1800941 (2018).
23. Rivnay, J. et al. High-performance transistors for bioelectronics through tuning of channel thickness. *Sci. Adv.* 1, e1400251 (2015).
24. Tarabella, G. et al. A single cotton fiber organic electrochemical transistor for liquid electrolyte saline sensing. *J. Mater. Chem.* 22, 23830–23834 (2012).
25. Lin, P., Yan, F. & Chan, H. L. W. Ion-sensitive properties of organic electrochemical transistors. *ACS Appl. Mater. Interfaces* 2, 1637–1641 (2010).
26. Ghittorelli, M. et al. High-sensitivity ion detection at low voltages with current-driven organic electrochemical transistors. *Nat. Commun.* 9, 1441 (2018).
27. Lingstedt, L. et al. Monitoring of cell layer integrity with a current-driven organic electrochemical transistor. *Adv. Healthc. Mater.* 8, 1900128 (2019).
28. Klauk, H., Zschieschang, U., Pflaum, J. & Halik, M. Ultralow-power organic complementary circuits. *Nature* 445, 745–748 (2007).
29. Hong, K. et al. Aerosol jet printed, sub-2 V complementary circuits constructed from P- and N-type electrolyte gated transistors. *Adv. Mater.* 26, 7032 (2014).
30. Torricelli, F. et al. Ambipolar organic tri-gate transistor for low-power complementary electronics. *Adv. Mater.* 28, 284–290 (2016).
31. Porrazzo, R. et al. Water-gated n-Type organic field-effect transistors for complementary integrated circuits operating in an aqueous environment. *ACS Omega* 2, 1–10 (2017).
32. Sun, H. et al. Complementary logic circuits based on high-performance n-type organic electrochemical transistors. *Adv. Mater.* 30, 1704916 (2018).
33. Venkatraman, V. et al. Subthreshold operation of organic electrochemical transistors for biosignal amplification. *Adv. Sci.* 5, 1800453 (2018).
34. Braendlein, M., Lonjaret, T., Leleux, P., Badier, J. M. & Malliaras, G. G. Voltage amplifier based on organic electrochemical transistor. *Adv. Sci.* 4, 1600247 (2017).
35. Inal, S., Malliaras, G. G. & Rivnay, J. Benchmarking organic mixed conductors for transistors. *Nat. Commun.* 8, 1767 (2017).
36. Khodagholy, D. et al. High transconductance organic electrochemical transistors. *Nat. Commun.* 4, 2133 (2013).
37. Thiburce, Q., Giovannitti, A., McCulloch, I. & Campbell, A. J. Nanoscale ion-doped polymer transistors. *Nano Lett.* 19, 1712–1718 (2019).
38. Torricelli, F., Colalongo, L., Raiteri, D., Kovács-Vajna, Z. M. & Cantatore, E. Ultra-high gain diffusion-driven organic transistor. *Nat. Commun.* 7, 10550 (2016).
39. Romele, P., Ghittorelli, M., Kovács-Vajna, Z. M. & Torricelli, F. Ion buffering and interface charge enable high performance electronics with organic electrochemical transistors. *Nat. Commun.* 10, 3044 (2019).
40. Bernards, D. A. & Malliaras, G. G. Steady-state and transient behavior of organic electrochemical transistors. *Adv. Funct. Mater.* 17, 3538–3544 (2007).
41. Torricelli, F. et al. Transport physics and device modeling of zinc oxide thin-film transistors - part ii: contact resistance in short channel devices. *IEEE Trans. Electron. Dev.* 58, 3025–3033 (2011).
42. Ofran, Y., Lavi, D., Opher, D., Weiss, T. A. & Elinav, E. Fatal voluntary salt intake resulting in the highest ever documented sodium plasma level in adults (255 mmol L^{-1}): a disorder linked to female gender and psychiatric disorders. *J. Intern. Med.* 256, 525–528 (2004).
43. Wu, X. et al. Ionic-liquid doping enables high transconductance, fast response time, and high ion sensitivity in organic electrochemical transistors. *Adv. Mater.* 31, 1805544 (2019).
44. Macchia, E. et al. Ultra-sensitive protein detection with organic electrochemical transistors printed on plastic substrates. *Flex. Print. Electron* 3, 034002 (2018).
45. Pappa, A.-M. et al. Organic transistor arrays integrated with finger-powered microfluidics for multianalyte saliva testing. *Adv. Healthc. Mater.* 5, 2295–2302 (2016).
46. Bernards, D. A. et al. Enzymatic sensing with organic electrochemical transistors. *J. Mater. Chem.* 18, 116–120 (2008).
47. Berto, M. et al. Label free urea biosensor based on organic electrochemical transistors. *Flex. Print. Electron* 3, 024001 (2018).

48. Pappa, A. M. M. et al. Direct metabolite detection with an n-type accumulation mode organic electrochemical transistor. *Sci. Adv.* **4**, eaat0911 (2018).

49. Coppedè, N. et al. Human stress monitoring through an organic cotton-fiber biosensor. *J. Mater. Chem. B* **2**, 5620–5626 (2014).

50. Lin, P., Luo, X., Hsing, I.-M. & Yan, F. Organic electrochemical transistors integrated in flexible microfluidic systems and used for label-free DNA sensing. *Adv. Mater.* **23**, 4035–4040 (2011).

51. Berto, M. et al. EGOFET peptide aptasensor for label-free detection of inflammatory cytokines in complex fluids. *Adv. Biosyst.* **2**, 1700072 (2018).

52. White, S. P., Frisbie, C. D. & Dorfman, K. D. Detection and sourcing of gluten in grain with multiple floating-gate transistor biosensors. *ACS Sens* **3**, 395–402 (2018).

53. Hai, W. et al. Human influenza virus detection using sialyllactose-functionalized organic electrochemical transistors. *Sens. Actuators, B Chem.* **260**, 635–641 (2018).

54. Berto, M. et al. Label free detection of plant viruses with organic transistor biosensors. *Sens. Actuators B Chem.* **281**, 150–156 (2019).

55. Macchia, E. et al. Single-molecule detection with a millimetre-sized transistor. *Nat. Commun.* **9**, 3223 (2018).

56. Li, Y., Yang, C. & Guo, X. Single-molecule electrical detection: a promising route toward the fundamental limits of chemistry and life science. *Acc. Chem. Res* https://doi.org/10.1021/acs.accounts.9b00347 (2019).

57. Wu, Y., Xiao, Y., Wang, X., Li, X. & Wang, Y. Chirality discrimination at the single molecule level by using a cationic supermolecule quasi-gated organic field effect transistor. *ACS Sens* **4**, 2009–2017 (2019).

58. Macchia, E. et al. Label-free and selective single-molecule bioelectronic sensing with a millimeter-wide self-assembled monolayer of anti-immunoglobulins. *Chem. Mater.* **31**, 6476–6483 (2019).

59. Macchia, E. et al. Selective single-molecule analytical detection of C-reactive protein in saliva with an organic transistor. *Anal. Bioanal. Chem.* **411**, 4899–4908 (2019).

60. Picca, R. A. et al. Ultimately Sensitive Organic Bioelectronic Transistor Sensors by Materials and Device Structures' Design. *Adv. Funct. Mater.* **30**, 1904513 (2020).

61. Macchia, E. et al. About the amplification factors in organic bioelectronic sensors. *Mater. Horiz.* **7**, 999 (2020).

62. Gkoupidenis, P., Koutsouras, D. A. & Malliaras, G. G. Neuromorphic device architectures with global connectivity through electrolyte gating. *Nat. Commun.* **8**, 15448 (2017).

Acknowledgements

Author contributions

P.R. fabricated and measured the OECTs, ion selective membranes, and amplifiers. P.G. supported and supervised the fabrications and measurements. D.K. fabricated the OECTs. K.L. supported the device fabrication. P.W.M.B., Z.M.K.V. and F.T. supervised the project. F.T. conceived the idea and designed the experiments. P.R. and F.T. wrote the paper. All the authors revised and commented on the paper.

Competing interests

The authors declare no competing interests.

Additional information

Supplementary information is available for this paper at https://doi.org/10.1038/s41467-020-17547-0.

Correspondence and requests for materials should be addressed to F.T.

Peer review information *Nature Communications* thanks Nicola Coppedè and the other, anonymous, reviewer(s) for their contribution to the peer review of this work. Peer reviewer reports are available.

Reprints and permission information is available at http://www.nature.com/reprints

Publisher's note Springer Nature remains neutral with regard to jurisdictional claims in published maps and institutional affiliations.